Volume 1 | Number 1 | Jan 2013 | Pages 1–100

CrystEngComm

www.rsc.org/crystengcomm

ROYAL SOCIETY OF CHEMISTRY

This is an *Accepted Manuscript*, which has been through the Royal Society of Chemistry peer review process and has been accepted for publication.

Accepted Manuscripts are published online shortly after acceptance, before technical editing, formatting and proof reading. Using this free service, authors can make their results available to the community, in citable form, before we publish the edited article. We will replace this *Accepted Manuscript* with the edited and formatted *Advance Article* as soon as it is available.

You can find more information about *Accepted Manuscripts* in the **Information for Authors**.

Please note that technical editing may introduce minor changes to the text and/or graphics, which may alter content. The journal's standard **Terms & Conditions** and the **Ethical guidelines** still apply. In no event shall the Royal Society of Chemistry be held responsible for any errors or omissions in this *Accepted Manuscript* or any consequences arising from the use of any information it contains.

Unusual Upconversion Emission from Single NaYF$_4$: Yb^{3+}/Ho^{3+} Microrod with NIR Excitation

Wei Gao, Hairong Zheng[*], Qingyan Han, Enjie He, Ruibo Wang

School of Physics and Information Technology, Shaanxi Normal University, Xi'an

710062, China

*Corresponding author: Hairong Zheng

E-mail: hrzheng@snnu.edu.cn

Abstract

Rare earth ions doped upconversion materials show great potential applications in optical and optoelectronic devices due to these novel optical properties. In this work, the NaYF$_4$:Yb^{3+}/Ho^{3+} microrods have been successfully prepared by hydrothermal method assisted with EDTA (ethylenediaminetetraacetic acid). The time controlled experiments are carried out and the grow mechanism of the microrods of dissolve-recrystallization are proposed. It is important that the unusual upconversion emissions with a candy-like pattern from a single NaYF$_4$: Yb^{3+}/Ho^{3+} microrod can be detected with a confocal microscopy under NIR 980 nm excitation. The influence of particle number on the UC emission spectra and overall luminescence color are investigated systematically. Noted that the multicolor emission from the single NaYF$_4$:Yb^{3+}/Ho^{3+} microrod can be successfully obtained only by adjusting the excitation strength or the size of the microrod. The present study is of great importance in the multicolor tuning of RE doped NaYF$_4$ nano/micro-materials as well as in the understanding of the up-mechanism. In addition to, the luminescence from a

single micropaticle can provide more precise spectra information for three-dimensional display and biological label.

Keywords: Single NaYF$_4$: Yb^{3+}/Ho^{3+} microrod; Upconversion luminescence emission; Hydrothermal method

1 Introduction

Rare-earth (RE)-doped upconversion (UC) luminescent materials have potential applications in display,[1] solar cell,[2,3] solid-state laser,[4] and biological labeling and imaging due to their novel electronic structure and optical properties.[5–7] In most cases, host matrix materials with low phonon energy are employed because of the minimized quenching effect.[8–12] Among these materials, the NaYF$_4$ crystal is considered as the most efficient UC emission host matrix because of its low phonon energy and optical transparency over a wide spectral range.[13–15] Yb^{3+}/Er^{3+} co-doped NaYF$_4$ nanocrystals have been successfully applied in DNA detection,[16] avidin,[17] and imaging of cells and tissues.[18] Compared with the RE-doped nanocrystals, microcrystals can emit stronger UC fluorescence because of their smaller surface-to-volume ratio and lower density of surface quenching centers,[19, 20] which present great application potential in three-dimensional display technology, micro-optoelectronic devices, and solar cells. Several efforts have been given for synthesizing RE-doped NaYF$_4$ crystals through various methods, including hydrothermal method,[21] solvothermal routes,[22] high-temperature thermal decomposition of trifluoroacetate precursors and liquid–solid two-phase approaches.[23,24] Compared with the other methods, the hydrothermal method is rather effective and convenient for preparing inorganic

materials with controllable structures, morphologies and sizes.[25-27]

The trivalent Ho^{3+} ion is considered as an intriguing active ion for UC emission because of its broad fluorescence spectrum, ranging from vacuum ultraviolet to infrared light.[28, 29] Generally, the UC emission from Yb^{3+} and Ho^{3+} co-doped systems results in an intense green emission accompanied by a weak red emission. A predominantly green UC emission has been frequently observed in Ho^{3+}-doped low phonon energy inorganic materials.[30, 31] However, the enhancement on the blue and red emission is rarely reported from Yb^{3+} and Ho^{3+} co-doped UC process. Li and his coworkers have observed that the $^5F_3 \rightarrow {}^5I_8$ transition gradually became stronger with increasing pump power density in $NaYF_4$: $Yb^{3+}/Ho^{3+}/Ce^{3+}$ nanorods because of the efficient energy transfer between Ce^{3+} and Ho^{3+}.[32] Enhanced red UC emission has been observed in the LaF_3: Yb^{3+}/Ho^{3+} nanoparticles because of the presence of organic ligands that stabilize the nanoparticles and quench green emission,[33] and from the high phonon energy host of the YVO_4 nanocrystals with high Yb^{3+} concentration.[34]

In the current work, hexagonal phase $NaYF_4$: Yb^{3+}/Ho^{3+} microrods have been synthesized by hydrothermal method, using EDTA as a chelator for controlling the particle size and morphology. The possible formation mechanism is systematically studied. The influence of particle number on the UC emission spectrum color is discussed in detail under NIR excitation at 980 nm with a confocal microscopy setup. The UC emission intensity and spectrum color from single microrod with different excitation powers and particle sizes are also investigated.

2   Experimental details

2.1 Synthesis of NaYF$_4$: 20%Yb^{3+}/2%Ho^{3+} Microparticles

All chemicals used in the current study are analytic grade and used directly without further purification. Y(NO$_3$)$_3$·6H$_2$O, Yb(NO$_3$)$_3$·6H$_2$O and Ho(NO$_3$)$_3$·6H$_2$O are obtained by dissolving Y$_2$O$_3$, Yb$_2$O$_3$ and Ho$_2$O$_3$ (99.99%, Sigma-Aldrich) with nitric acid first, respectively. The solution is stirred at 60 ^{o}C for several hours to remove excess nitric acid. Then it is dissolved in deionized water to form RE((NO$_3$)$_3$) solution. NH$_4$HF$_2$ (98.0%), NaF (98.0%), and EDTA (99.0%) with analytical grade are supplied by the Tianjin chemical reagent factory.

   NaYF$_4$: 20%Yb^{3+}/2%Ho^{3+} microparticles are synthesized by hydrothermal method for which the detailed process is given in the reference.[35] The preparation process is presented as follows: Firstly, the water solution of RE(NO$_3$)$_3$ (0.5 M, RE=Y, Yb and Ho), deionized water and EDTA are mixed to form a chelating complex solution under vigorous stirring about 40 min. Then the water solution of NaF (1.0 M) and NH$_4$HF$_2$ (1.0 M) are added into the chelating complex solution with vigorous stirring for about 20 min until it completely becomes white liquid. The pH value of the mixed solution was adjusted to 3 by adding diluted HNO$_3$ solution. Finally, the white liquid is slowly transferred into a 50 ml Teflon-lined autoclave and is heated at 200 ^{o}C for 24 h to get NaYF$_4$: 20%Yb^{3+}/2%Ho^{3+} microparticles. The specific size of NaYF$_4$: 20%Yb^{3+}/2%Ho^{3+} microparticles are obtained by adjusting the reactant ratio at the same reaction temperature, time and pH value. A summary of these parameters is given in the Table 1. The precipitates are separated by centrifuging, wash with

deionized water and ethanol for several times, and finally dried at $60\,^{\circ}C$ for 12 h.

2.2 Characterization

The powder x-ray diffraction (XRD) pattern is measured by a D/Max2550VB+/PC x-ray diffraction meter with Cu Kα (40 kV, 40 mA) irradiation ($\lambda = 0.15406$ nm). The 2θ angle of the XRD spectra is recorded at a scanning rate of $8° \ min^{-1}$. The morphology of the particles is characterized by the scanning electron microscope (SEM, Quanta 200) operating at voltage of 20 kV. The Fourier transform infrared spectroscopy (FTIR) is measured using a Brucher EQUINX55 spectrometer. For spectroscopic measurement, Ti sapphire femtosecond laser (Mira-900) is employed as excitation sources. The spectrometer (SP2750i) with a spectral resolution of 0.008 nm is used for luminescence collection and detection. The confocal setup is built with an optical microscope (OLYMPUS-BX51), and the corresponding magnifications are 100, 500 and 1000. A proper notch filter is placed in front of the entrance of the monochromator to block the scattering light. All of the spectroscopic measurements are carried out at room temperature.

3   Results and discussion

3.1 Structure and morphology of NaYF$_4$: 20%Yb^{3+}/2%Ho^{3+} microparticles.

The typical XRD pattern and morphology of NaYF$_4$: Yb^{3+}/Ho^{3+} microcrystals are shown in Fig. 1. Strong and sharp diffraction peaks match well with the standard data (JCPDS card 28-1192) in the $P6_3$/m space group, which suggests that the prepared NaYF$_4$ microcrystals are pure hexagonal phase with cell parameters of $a = 5.961$ nm and $c = 3.520$ nm. No obvious extra diffraction peaks are detected. The

microparticles display uniform distribution and rod-like morphologies. Their diameter and length are about 4 μm and 12 μm, as shown by SEM in Fig. 1b. Fig. 3c is the EDS of $NaYF_4$: Yb^{3+}/Ho^{3+} microrods, in which elements of Na, Y, Yb, F and Ho are clearly presented. The XRD patterns and SEM images of Yb^{3+}/Ho^{3+} microrods with different sizes are shown in Fig. S1 and S2 of the supporting information.

3.2 Growth mechanism of $NaYF_4$: 20%Yb^{3+}/2%Ho^{3+} microrods

To better understanding the formation mechanism of $NaYF_4$: Yb^{3+}/Ho^{3+} microrods, we systematically investigated various samples by quenching the reaction at different time intervals. Fig. 2 shows the XRD patterns of the intermediates obtained at different reaction times, the standard date of the cubic $NaYF_4$ (JCPDS No. 77-2042), and the hexagonal $NaYF_4$ (JCPDS No. 28-1192) phase for comparison. Different XRD patterns are obtained at different reaction periods. Only the cubic phase $NaYF_4$ crystals are obtained for 1 h of reaction time, as shown in Fig. 2a. When the reaction time is increased to 2 h, the hexagonal phase $NaYF_4$ crystal emerges, except for the cubic one, as shown in Fig. 2b. This result reveals that the samples transform partially from the cubic phase to the hexagonal phase with further reaction. Pure hexagonal $NaYF_4$ crystals are obtained when the reaction time is prolonged to 8 h. The intensities of the diffraction peaks are significantly increased with prolonged reaction time, indicating that the crystallinity of the sample increases with further reaction. Notably, the XRD patterns also indicate some differences in relative intensities based on (100) and (101), indicating the possibility of different preferential growth

orientation. The above analyses have indicated that the crystal evolves from the cubic

phase to the hexagonal phase, consistent with a previous report.[36]

The morphological evolution of the $NaYF_4$: Yb^{3+}/Ho^{3+} microrods are investigated

by SEM. A series of SEM images of $NaYF_4$: Yb^{3+}/Ho^{3+} microcrystals with different

reaction times are shown in Fig. 3. The crystallite aggregates present an irregular

spherical morphology with a short reaction time (1–2 h) (Figs. 3a and b). When the

reaction time is extended to 4 h, two different morphologies appear, which include

microrods and flower-like microsphere having small nanoparticles on the surface (Fig.

3b). After 8 h of hydrothermal reaction, the microrods and flower-like microspheres

with petals become much larger, and the nanopaticles on their surface almost

disappeared (Fig. 3c). However, as the reaction time reaches to 14 h, the flower-like

microspheres tend to decompose to form microrods, as shown in Fig. 3d. When the

reaction time is prolonged to 24 h, the flower-like microstructures completely

disappeared, and the uniform microrods with smooth surface are obtained, as shown

in Fig. 3f.

The possible morphology evolution mechanism of $NaYF_4$: Yb^{3+}/Ho^{3+} microrods

can now be addressed as shown in Fig. 4. It is evident that the microrods can be

formed through two different growth processes including one-step and two-step

process. The detailed formation processes are discussed as follows: At the beginning,

the EDTA will reacts with Ln^{3+} (Ln=Y, Yb and Ho) to form a stable Ln-EDTA

complex. With the increase of temperature and time under hydrothermal condition,

the Ln^{3+} will be slowly released into the solution and react with Na^+ and F^- to form the

NaYF$_4$ nuclei, subsequent these nuclei can only grow into irregular cubic phased

NaYF$_4$ nanoparticles when the reaction time up to 1 h. The cubic NaYF$_4$ nanoparticles

have isotropic unit cell, leading an isotropic growth to form spherical particles and

minimize the surface energy of the crystal facets. When the reaction time up to 2 h,

the cubic phase NaYF$_4$ nanoparticles are shown two kinds of different growth trends.

A part of unstable cubic phase NaYF$_4$ nanoparticles firstly dissolved and then formed

the thermodynamic stability hexagonal phase NaYF$_4$ crystal nucleus. With the

reaction time is prolonged to 4 h, NaYF$_4$ rod-like structures with a preferential growth

orientation continue through a dissolution-renucleation process to form final stable

hexagonal phase NaYF$_4$: Yb^{3+}/Ho^{3+} microrods with smooth surface. Another part of

cubic phase NaYF$_4$ nanoparticles congregate together forming polyhedral aggregates

with lots of nanoparticles on the surface. When aggregation reach to the key size of

phase transition with time prolonging, phase transition firstly occurred on the surface

of polyhedral aggregation, resulting in forming flower-like polyhedral spheres with

lots of petals instead of polyhedral by a growth along the [0001] direction of growing

point on the surface of polyhedron.[37] The flower-like ball cores and surrounding

solution can provide the nutrient element for growth of the petals. Therefore, with

further reaction, the NaYF$_4$: Yb^{3+}/Ho^{3+} microrods grow preferentially along the [0001]

direction, leading to the formation of 1D prismatic microrods. While the polyhedron

spheres with the big petals will dissolve until to disappear by Ostwald ripening due to

the weak crystallinity relative to its lateral branch(rods).[38] Finally, the individual

unification short microrods are obtained. The two kinds of different forming

mechnisms of microrods are shown in Fig. 4.

3. 3 UC fluorescence properties of NaYF$_4$: 20%Yb^{3+}/2%Ho^{3+} microrods.

3. 3. 1 The influence of particle number on UC emission

The UC luminescence emission of the NaYF$_4$: Yb^{3+}/Ho^{3+} microrods is carried out with a confocal setup. The emission spectra and luminescence photographs of the single NaYF$_4$: Yb^{3+}/Ho^{3+} microrod, double NaYF$_4$: Yb^{3+}/Ho^{3+} microrods and clustered NaYF$_4$: Yb^{3+}/Ho^{3+} microrods are shown in Fig. 5A under 980 nm excitation. The length of the microrods is about 12 μm. The emission bands centered at 484, 541, 579, 644 and 750 nm are assigned to the transitions of $^5F_3 \rightarrow ^5I_8$, $^5S_2(^5F_4) \rightarrow ^5I_8$, $^3K_7(^5G_4)$ $\rightarrow ^5I_6$, $^5F_5 \rightarrow ^5I_8$ and $^5S_2 \rightarrow ^5I_7$, respectively.[32] Fig. 5 A (a) shows that the single NaYF$_4$: Yb^{3+}/Ho^{3+} microrod exhibits pink candy-like UC emission pattern. It is noted that the red UC emission intensity of single microrod is much stronger than the green and blue emission. However, different luminescence emission pattern and color are observed in Fig. 5A (b)and (c) when the double and clustered microrods are excited in the same experimental condition, although the peak position is the same. Fig. 5B shows the peak area of blue, green, and red emission bands with different particle number. It can be seen that when the particle number is increased, the intensities of the three colors are apparently changed. The output colors for the samples also vary from pink to green with the increase of particle number, as shown in inset Fig. 5A. The color of luminescence is different because of different intensity ratio of blue to green to red in Fig. 5. These new phenomena suggest a possible influence of neighbored particles on the observation of luminescence emission.

To investigate the green (541 nm) and red (644 nm) UC luminescence emission mechanism, the pump-power dependent UC emission is measured. The points in Fig. 6a are what obtained from the experimental observation. A slope of 1.76 for the green emission ($^5S_2(^5F_4) \rightarrow {}^5I_8$) and 1.69 for the red emission ($^5F_5 \rightarrow {}^5I_8$) are obtained by fitting the experimental dates, suggesting that the green and red emissions are two-photo excitation processes in single $NaYF_4$: Yb^{3+}/Ho^{3+} microrod. This result is in agreement with the previous reports.[32] Fig. 6b displays the UC emission spectra of a single $NaYF_4$: Yb^{3+}/Ho^{3+} microrod that is excited with different laser powers. The UC emission intensity from a single particle decreases with the reduction of excitation power. Fig. 6c and d shows the peak area for the blue, green and red emission bands and the R/G ratio with different excitation power. The intensities of the three colors and the R/G ratio are obviously changed when the excitation power is reduced. The luminescence colors of the single $NaYF_4$: Yb^{3+}/Ho^{3+} microrod change from pink to green is presented in the inset of Fig. 6b. The phenomena can not be observed in multiple microrods. The result tells us that the UC luminescence properties of a single $NaYF_4$: Yb^{3+}/Ho^{3+} microrod can be tuned by adjusting the excitation power.

During the experimental observation, we have noticed that the overall UC luminescence color from the single $NaYF_4$: Yb^{3+}/Ho^{3+} microrod, double and clustered $NaYF_4$: Yb^{3+}/Ho^{3+} microrods are different under the same experimental conditions. To explore the reason behind this phenomenon, the transition process must be examined. Fig. 7 shows the proposed UC energy transfer process of Yb^{3+} and Ho^{3+} under 980 nm excitation. Since Yb^{3+} ion has a larger absorption cross section for

infrared light, longer excited state lifetime and higher doping concentration than that of Ho^{3+} ions. Thus, the main pathway to populate the upper emitting states is the energy transfer from Yb^{3+} ions to Ho^{3+} ions but not the excited state absorption. According to the energy level diagram, the proposed UC mechanism that produces the blue, green and red emissions is as follows: First, the ground state $^5I_8$ is excited to $^5I_6$ via energy transfer (ET) from the Yb^{3+} ions to the Ho^{3+} ions. the $^5I_7$ state is then populated through nonradiative relaxations of the $^5I_6$ state. The $^5I_6$ state is promoted to the $^5S_2(^5F_4)$ state by ET from the excited Yb^{3+} ions. When the $^5S_2(^5F_4)$ state decays to the ground the $^5I_8$ state and to the $^5I_7$ state by radiative relaxation, the green (541 nm) and the NIR (750 nm) UC emissions can be generated. The $^5F_5$ state can be populated by nonradiative relaxations of the $^5S_2(^5F_4)$ states or from the $^5I_7$ state through ET from the Yb^{3+} ions to the Ho^{3+} ions, which contribute to the red UC emission at 644 nm. Subsequent Ho^{3+} can be further promoted to $^3K_7(^5G_4)$ states from the $^5F_5$ state the by ET from excited Yb^{3+} ions. Then the $^5F_3$ state can be populated via nonradiative relaxations from the $^3K_7(^5G_4)$ states. The blue UC emission is produced when the $^5F_3$ state comes back to the ground state, However, at the very small excitation power, the $^3K_7(^5G_4)$ states is very difficult to populate using ET from the excited Yb^{3+} ions. Thus the strong blue and weak yellow emissions cannot be observed (Fig. 6b).

As presented in Fig. 5, the R/G ratio of the single microrod is higher than that from the clustered microrods, and the luminescence emission pattern and color are different. This phenomenon can be explained in the following way according to the proposed UC mechanisms. First, the power density of the single microrods stimulated by laser

are bigger than that multiple microrods, which due to the doped ions for the single

microrod system are into or very closer to the range of the excitation laser radiation.

The energy absorption by the ions and energy transfer of Yb^{3+} should be very intense.

Therefore, Ho^{3+} ions can easily obtain more energy transfer and great probability to

go up to higher excited states. The blue emission then can be much stronger.

Meanwhile, the cross-relaxation derived from Ho^{3+}, such as $^5S_2(^5F_4)(Ho^{3+})+^5I_7(Ho^{3+})$

$\rightarrow$ $^5I_6(Ho^{3+})+^5F_5(Ho^{3+})$ and $^5F_2(Ho^{3+})+^5I_8(Ho^{3+}) \rightarrow$ $^5F_5$ $(Ho^{3+})+^5F_7$ (Ho^{3+}), can be

generated when the more energy transfer from Yb^{3+} to Ho^{3+} ions under intense

excitation power (Fig. 7). These cross-relaxations will effectively increase the red

emission and quench the green one. In order to investigate the high R/G ratio of single

microrods is due to cross-relaxations derived from Ho^{3+}. We consider that some

measurements, where the UC luminescent properties of single $NaYF_4$: Yb^{3+}/Ho^{3+}

microrod as a function of Yb^{3+} concentration and excitation power are also studied

under 980 nm excitation, respectively. Fig. 8a and b displays the UC emission spectra

and R/G ratio of a single $NaYF_4$: $2\%Ho^{3+}$ microrod codoped with different Yb^{3+}

concertration. It is found that the R/G ratio of a single $NaYF_4$ microrod is increased

from 0.58 to 2.37 with the the Yb^{3+} concentration increasing from 5% to 40%. And

the UC emission intensity of a single $NaYF_4$ microrod frist increases and then

decreases as Yb^{3+} concentration. Fig.8c and d show pump-power dependence of the

green and red UC emission of single $NaYF_4$: Yb^{3+}/Ho^{3+} microrods with different Yb^{3+}

concentration. As shown in the value of n decreases with increasing the Yb^{3+}

concentration in the range of 1 and 2. As is well known, for the two-photon processes,

n should be equal to or close to 2. However, the values of *n* for the green and red emissions in single $NaYF_4$: $2\%Ho^{3+}$ microrod system are gradually deviated from 2, which could be mainly due to the competition between different decay channels with the intermediate excited states.[39] In fact, cross-relaxation process of $^5S_2(^5F_4)(Ho^{3+})+^5I_7(Ho^{3+}) \rightarrow ^5I_6(Ho^{3+})+^5F_5(Ho^{3+})$ at high Yb^{3+} concentration is rampant. It is noticed that blue emission of $^5F_3 \rightarrow ^5I_8$ increases when Yb^{3+} concentration increases from 5% to 20% (Fig. 8a), which indicate the cross-relaxation process $^5F_2(Ho^{3+})+^5I_8(Ho^{3+}) \rightarrow ^5F_5 (Ho^{3+})+^5F_7 (Ho^{3+})$ is weak. Therefore, the higher R/G ratio from single $NaYF_4$ microrod is mainly due to the cross-relaxation process of $^5S_2(^5F_4)(Ho^{3+})+^5I_7(Ho^{3+}) \rightarrow ^5I_6(Ho^{3+})+^5F_5(Ho^{3+})$ when the Yb^{3+} concentration is 20%. The Similar phenomena are also observed in $NaYF_4$: Yb^{3+}/Er^{3+} microcrystals.[39] The decrease of UC emission intensity may be due to concentration quenching. Second, for the double and clustered microrods, as shown in the Fig. 5b and c, not all of the luminescence ions are within the area that directly radiated by the excitation laser. The microrods outside of the laser radiation are excited by the scattered light, thus the actual excitation energy is low. Based on the Fig. 5, when the excitation power is low, a green emission accompanied by a weak red emission is observed and the blue emission is reduced too. The output colors of the single $NaYF_4$ microrod are close to green. Thus the R/G ratio and output colors of the single microrod is different the double and clustered microrods.

3. 3. 2 The influence of particle size on UC emission

The size-dependence of the UC emission from a single $NaYF_4$: $20\%Yb^{3+}/2\%Ho^{3+}$

microirod has also been investigated too. The XRD patterns and SEM images of the NaYF$_4$ microrods with different size are shown in Fig. S1 and Fig. S2. Fig. 9 shows the UC emission spectra, R/G ratio, the peak area of blue, green and red emission, and CIE chromaticity diagram of the three single microrod samples with different sizes. The lengths for three particles are 20, 12 and 8 μm, respectively. The excitation light is NIR at 980 nm. The luminescence color and emission intensity are also found to be different for different particle sizes. The UC emission intensity decreases with the decrease of the particle size. Compared with smaller microrods, bigger microrods have the smaller surface-to-volume ratio and high crystallinity, which may lead to the significant luminescence enhancement. Moreover, the intensity of luminescence emission of lanthanide-doped materials is known to depend on the orientation of the unique crystal axis relative to the polarization vector of the incident light.[40-41] The preferred growth trend of big microrods along the [0001] axes is stronger, which benefits the increase of the luminescent efficiency. Therefore, the big microrods exhibit strong UC emission. Fig. 9C shows the peak area for the blue, green and red emission bands of single microrod with different sizes. The relative intensities of the blue, green and red bands change with the decrease in the microrod size. When the microrod size is 8 μm, the intensities of the three colors are closest to whiter than that the others, which can be confirmed by the corresponding CIE chromaticity coordinates is shown in Fig 9D. This indicates that the emission intensity ratio of blue, green and red has been tuned by adjusting the size of microrods.

The R/G ratio increases from 1.03 to 2.14 with the lengths of the microrod increasing

from 8 μm to 20 μm as presented in Fig. 9B. The increase in the R/G ratio might be due to the increase of the nonradiative transition probability of $^5S_2(^5F_4) \rightarrow {}^5F_5$ and $^5I_6 \rightarrow {}^5I_7$, which is most probably ascribed to the different amounts of organic ligands on the microrod surface.[42-43] In the synthesis process of the $NaYF_4$: Yb^{3+}/Ho^{3+} microrods, EDTA is employed as a chelator to control the particle size and morphology. Thus, some organic molecules can remain on the surface of the samples, their vibrational states can provide some extra pathways for the nonradiative recombination of the upconversion states.[44] FTIR spectroscopy can help us to identify the capping ligands on the surface of microrods. The observed FTIR spectra from the microrods with different sizes are shown in Fig. 10. The $-CH_2-$ (2850 cm^{-1}) stretching, $-CH_2-$ (1400 cm^{-1}) bending, C-O (1091 cm^{-1}) stretching and -COO- (1640 cm^{-1}) stretching and -OH (3400 cm^{-1}) vibrations have been observed,[45] which proves the existence of EDTA on the surface of the microrods. It is also found that the big microrods present stronger FTIR signal than that small ones. According to the energy level diagram and UC mechanism, multiphonon nonradiative relaxations of $^5S_2(^5F_4) \rightarrow {}^5F_5$ and $^5I_6 \rightarrow {}^5I_7$ should be very weak. The reason being is that their energy gaps are about 3400 cm^{-1} and 2800 cm^{-1}, which are about eight times higher than the phonon energy of the $NaYF_4$ matrix that is about 370 cm^{-1}.[46] According to the Fig. 10, the hydroxyl groups (2700-3600 cm^{-1}) possess high-energy vibration modes that would strongly quench the excited states of Ho^{3+} ions and accelerate the multiphonon relaxations of $^5S_2(^5F_4) \rightarrow {}^5F_5$ and $^5I_6 \rightarrow {}^5I_7$, leading to the population increase of the intermediate states, and finally changing the relative intensity of red and green

emissions. Thus, we suggest that higher R/G ratio from big microrods is due to more organic ligands at the surface of the samples. The output color of the small single microrod is much closer to white can be attributed to particle size and excitation power. For the smaller single microrod, the luminescent ions in host lattice are closer to the range of the excitation laser radiation than that the bigger one in the same experimental condition. Ho^{3+} ions will absorb more energy through energy transfer of Yb^{3+} ions. Thus, the Ho^{3+} ions can easily go up to $^3K_7(^5G_4)$ excited states. The blue emission intensity then can be enhanced. The output color from the smaller microrods is more close to the white. The schematic diagram of the excitation process of a single microrod with different sizes is shown in Fig.10B.

4   Conclusion

The $NaYF_4$:Yb^{3+}/Ho^{3+} microrods with control size have been successfully prepared by hydrothermal approach assisted with EDTA. The grow mechanism of the microrods of dissolve-recrystallization are proposed based on the time contol experiment. It is important that the strong upconversion emissions with a candy-like pattern from a single $NaYF_4$: Yb^{3+}/Ho^{3+} microrod can be detected with a confocal microscopy under NIR 980 nm excitation. Noted that the multicolor emission and R/G ratio from the single $NaYF_4$:Yb^{3+}/Ho^{3+} microrod can be successfully tuned only by adjusting the excitation strength or the size of the microrod. The tuning mechanism is revealed by a series of experiment. The emission intensity and R/G ration dependence on the particles size is own to the change of the surface-to-volume ratio,

high crystallinity, growth trend and vibration of organic molecules. The present study is of great importance in the multicolor tuning of RE doped $NaYF_4$ nano/micro-materials as well as in the understanding of the up-mechanism. In addition to, the luminescence from a single micropaticle can provide more precise spectra information for three-dimensional display and biological label. The formation of Candy-like emission pattern and the mechanism behind it will be published in a separate work.

Acknowledgements

References

1 E. Downing, L. Hesselink, J. Ralson, R. MacFarlane, *Science*, 1996, 273, 1185-1189.

2 T. Trupke, MA. Green, P. Würfel, *J. APPL. Phys*, 2010, 94, 1919-1922.

3 D. Chen, Y. Wang and M. Hong, *Nano Energy*, 2012, 1, 73-90.

4 M. H. Huang, S. Mao, H. Feick, H. Yan, Y. Wu, H. Kind, E. Weber, R. Russo and P. Yang, *Science*, 2001, 292, 1897-1899.

5 F. Wang, X. G. Liu, *Chem. Soc. Rev*, 2009, 38, 976-989.

6 T. S Yang, Y. Sun, Q. Liu, W. Feng, P.Y.Yang, F.Y. Li, *Biomaterials*, 2012, 33, 3733-3742.

7 F.van de Rijie, H. Zijlmans, S. Li, T. Vail, K. A. Raap, R. S. Niedbala, H. J. Nat

Tanke, *Biotechnol*, 2001, 19, 273-6.

8   D. L. Gao, H. R. Zheng, X. Y. Zhang, Z. X. Fu, Z. L. Zhang, Y. Tian, M. Cui, *Appl Phys. Lett*, 2011, 98, 011907.

9   Sri Sivakumar Frank C J M van Veggel and R. Mati, *J. Am. Chem. Soc*, 2005, 127, 12464-12465.

10 M. F. Zhang, H. Fan, B. J. Xi, X. Y. Wang, C. Dong and Y. T. Qian, *J.Phys. Chem.C*, 2007, 111, 6652-6657.

11 S. Ahmad, P. G. Vijaya and R. Nagarajan, *Inorg Chem*, 2012, 51, 12748-12754.

12   K. Kramer, D. Biner, G. Frei and H. Gudel, *Chem. Mater*, 2004, 16, 1244-1251.

13   F. Zhang, Y. Wan, T. Yu, F. Zhang, Y. Shi , S. Xie, Y. Li, L. Xu, B. Tu, D. Zhao, *Angew. Chem. Int Ed*, 2007, 46, 7976-7979.

14   J. Tao, W. P. Qin, W. H. Di, R.Y.Yang, D. M. Liu, X. S. Zhai and G. S. Qin, *CrystEngComm*, 2012,14, 2302-2307.

15   W. Yu, W. Xu, H. W. Song, S. Zhang, *J.Name*, 2013,00,1-3.

16   L. Y. Wang, Y. D. Li, *Chem. Comm*, 2006, 24, 2557-2559.

17   L. Y. Wang, R. X. Yan, Z. Y. Huo, L. Wang, J. Zeng, J. Bao, X. Wang, Q. Peng, Y. D Li, *Angew. Chem, Int Ed*, 2005, 44, 6054-6057.

18 S. F. Lim, R. Riehn, W. S. Ryu, N. Khanarian, C. K. Tung, T. Dank, R. H. Austin, *Nano Lett*, 2006, 6, 169.

19   A. Yin, Y. Zhang, L. Sun, C. Yan, *Nanoscale*, 2010, 2, 953-959.

20   F. Wang, J. Wang, X. G. Liu, *Angew. Chem, Int Ed.*, 2010, 49, 7456-7460.

21   L. Y.Wang, Y. D. Li, *Chem. Mater*, 2007, 19, 727-734.

22   D. L. Gao, X. Y. Zhang, H. R. Zheng, P. Shi, L. Li, Y. W. Ling, *Dalton. Trans*,

 2013, 42, 1834-1841.

23   J. C. Boyer, F. Vetrone, L. A. Cuccia, J. A. Capobianco, *J. Am. Chem. Soc*, 2006,

128, 7444-7445.

24   Y Wei, F. Q. Lu, X. R. Zhang and D. P. Chen, *Chem. Mater*, 2006, 18,

5733-5737.

25   N. Niu, P. P. Yang, F. He, Z. Xhang, S. L. Gai, C. X. Li, J. Lin, *J. Mater. Chem*,

2012, 22, 10889-10899.

26   M. Y. Ding, C. H. Lu, L. H. Cao, Y. R. Ni, Z. Z. Xu, *CrystEngComm*, 2013, 15,

8366-8373.

27   C. X. Li, J. Yang, Z. W. Quan, P. P. Yang, D. Y. Kong, J. Lin. *Chem. Mate*,

2007, 19, 4933-4942.

28   G. S. Qin, W. P. Qin, C. F. Wu, S. H. Huang, S. Zhao, J. S. Zhang, S. Z. Lu, *Opt.*

Commun, 2004, 242, 215-219.

29   H. Lin, Y. Y. Zhang, E. Y. B. Pun, *Spectrochim. Acta. A*, 2008, 71, 1547-1550.

30   X. X. Zhang, P. Hong, M. Bass, B. H. T, Chai. *Appl. Phys. Lett*, 1993, 63,

2606-2608.

31   T. Li, C. F. Guo, Y. M. Yang, L. Li, N. Zhang. *Acta. Materialia*, 2013, 61,

7481-7487.

32   G. F. Wang, P. Qing and Y. D. Li, *Chem. Eur. J*, 2010, 16, 4923-4931.

33   G. S. Yi, G. M. Chow. *J.Mater. Chem*., 2005, 15, 4460-4464.

34   R. Lisiecki, G. Dominiak-Dzik, W. Ryba-Romanowski, T. Lukasiewicz, *J.*

Appl .Phys, 2004, 96, 6323-6330.

35   J. L. Zhuang, L. F. Liang, H. H. Y. Sung, X. F. Yang, M. M. Wu, I. D. Williams,

S. H.Feng, Q. Su, *Inorg. Chem*, 2007, 46, 5404-5410.

36   D. L. Gao, X. Y. Zhang, W. Gao, *Appl. Mate.r Interfaces*, 2013, 5, 9732-9739.

37   Y. Wei, F. Q. Lu, X. R. Zhang, D. P. Chen, *Chem. Mater*, 2006, 18, 5733-5737.

38   N. Liu, D. Zhao, L. X. Yu, K. Z. Zheng, W. P. Qin. *Colloids and Surfaces A:*

*Physicochem. Eng. Aspect*s, 2010, 363,124-129.

39   D. L. Gao, X. Y. Zhang, H. R. Zheng, W. Gao, E. J. He, *J. Alloys. Comp*, 2013,

554, 395-399.

40   B. Wu, H. Chen, Z. Hua, Z. Liu, W. Huang, L. Zhang, J. Shi, *Appl. Phys. Lett*,

2004, 85, 4307-4309.

41   D. K. Ma, D. P. Yang, J. L. Jiang, P. Cai, S. M. Huang, *CrystEngComm*, 2010,

12(5), 1650-1658.

42   S. Wu, Y. Ning, J. Chang, W. Niu, S. Zhang, *CrystEngComm*, 2013, 15,

3919-3924.

43   S. Schietinger, L. D. S. Menezes, B. R. Lauritzen, O. Benson, *Nano. Lett*, 2009,

9, 2477-2481.

44   Y. Wang, L. Tu, J. Zhao and Y.Sun, *J. Phys. Chem. C*, 2009, 113, 7164-7169.

45 C. H. Lu, W. J. Huang, Y. R. Ni and Z. Z. Xu, *Mater. Res. Bull*, 2011, 46,

216-221.

46   J. F. Suyver, J. Grimm, M. K. Veen, D. Biner, K. W. Krämer and H. U. Güdel, *J.*

Lumin., 2006, 117,1-12.

Table

Table 1. The reactant concentration and correspongding size $NaYF_4$ microrods.

Sample	H_2O (ml)	$Y(NO_3)_3$ (ml)	$Yb(NO_3)_3$ (ml)	$Ho(NO_3)_3$ (ml)	NaF (ml)	NH_4HF_2 (ml)	EDTA (g)	Length and diameter (μm)
a	18.0	1.17	0.30	0.03	4.0	8.0	0.2848	*l*=21, *d*=5
b	21.0	0.78	0.20	0.02	3.0	6.0	0.1784	*l*=12, *d*= 4
c	24.0	0.38	0.10	0.01	2.0	4.0	0.0947	*l*=8, *d*=5

Figure
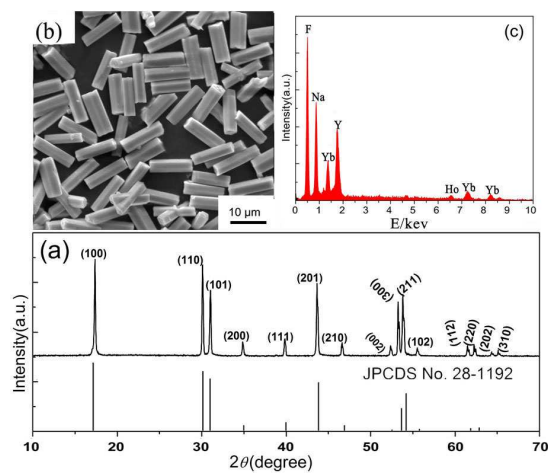
Fig. 1   XRD pattern (a), SEM image (b) and EDX spectrum (c) of NaYF$_4$: Yb^{3+}/Ho^{3+}

microrods
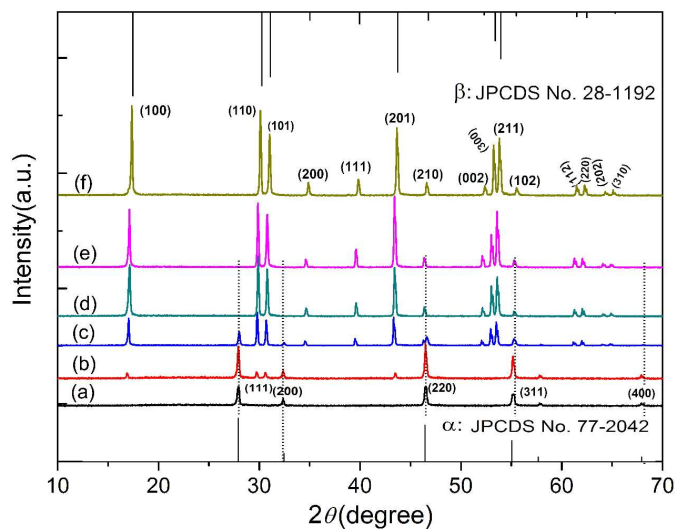
Fig. 2   The dependence of XRD patterns of NaYF$_4$: Yb^{3+}/Ho^{3+} microrods on the

hydrothermal reaction time. (a) 1 h, (b) 2 h, (c) 4 h, (d) 8 h, (e) 14 h, and (e) 24 h.
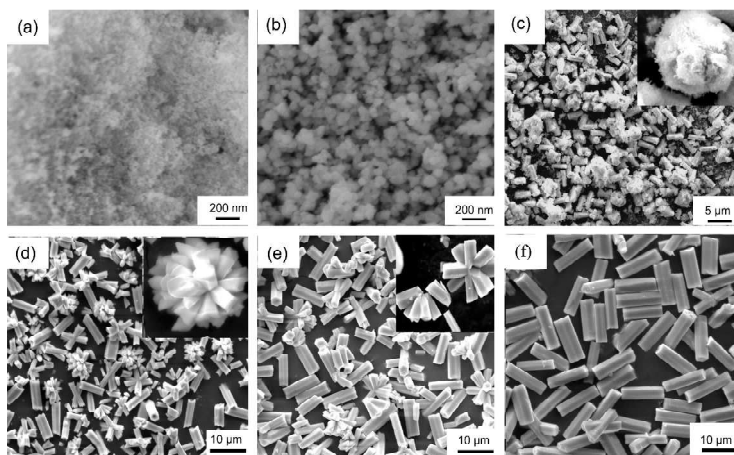
Fig. 3   SEM images of NaYF$_4$:Yb^{3+}/Ho^{3+} microrods obtain at 200 ^{o}C for different reaction time. (a) 1 h, (b) 2 h, (c) 4 h, (d) 8 h, (e) 14 h, (f) 24 h. The insets are corresponding high-magnification SEM images.
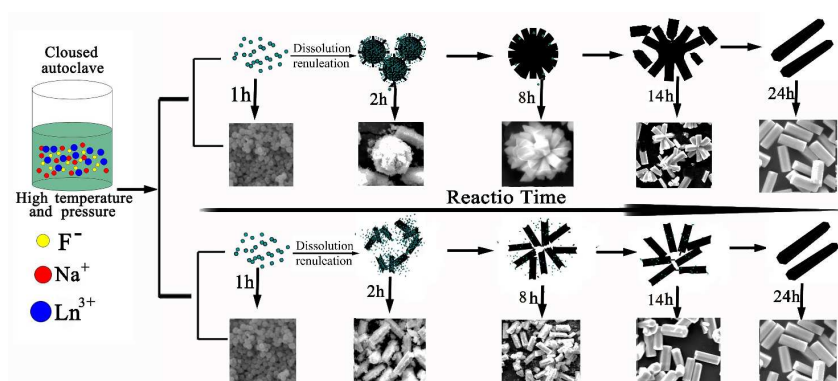
Fig. 4 Schematic diagram of the proposed formation of NaYF$_4$: Yb^{3+}/Ho^{3+} microrods.
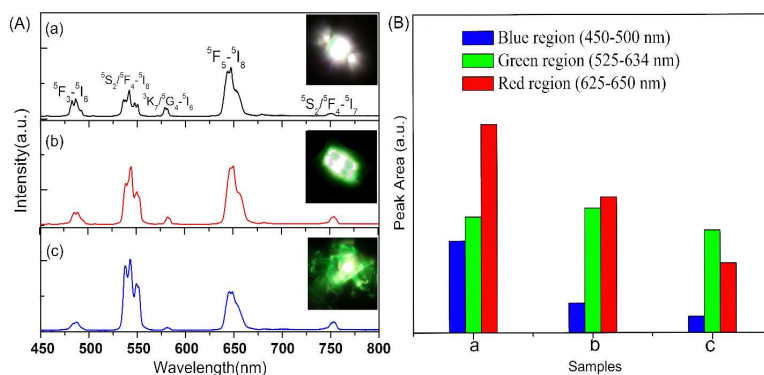
Fig. 5 (A) UC emission spectra and (B) the peak area of the blue, green and red

emission of single NaYF$_4$: Yb^{3+}/Ho^{3+} microrods (a), double NaYF$_4$: Yb^{3+}/Ho^{3+} microrods (b), clustered NaYF$_4$: Yb^{3+}/Ho^{3+} microrods (c) under 980 nm excitation. The insets show the corresponding luminescence photographs.
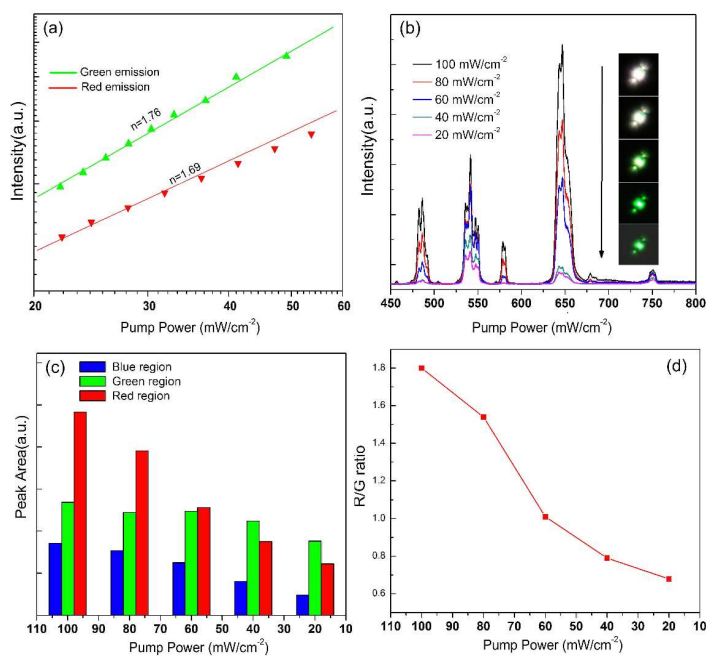
Fig. 6   (a) Pump power dependence of the green and red UC emission intensity. (b) UC emission spectra, (c) the peak area of the blue, green and red emission and (d) R/G ratio of NaYF$_4$:20%Yb^{3+}/2%Ho^{3+} MCs with length is 12 μm as a function of excitation power. The inset exhibits the corresponding luminescence photographs.
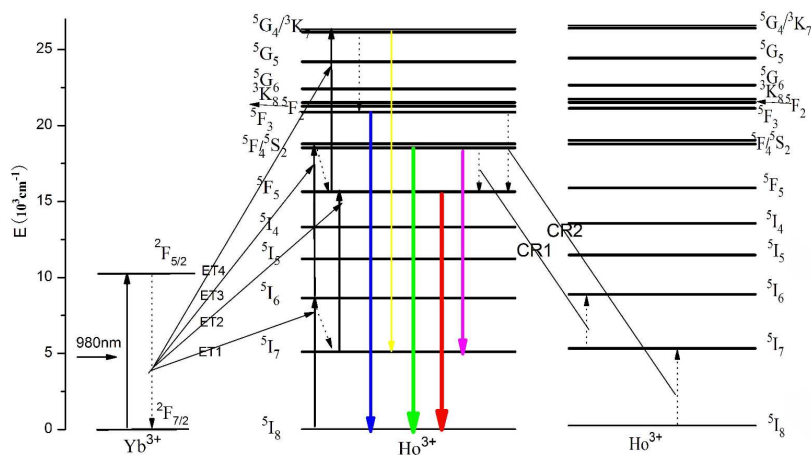
Fig. 7 Energy level diagrams and proposed energy transfer pathways for Ho^{3+} and Yb^{3+} codoped $NaYF_4$ microrods.

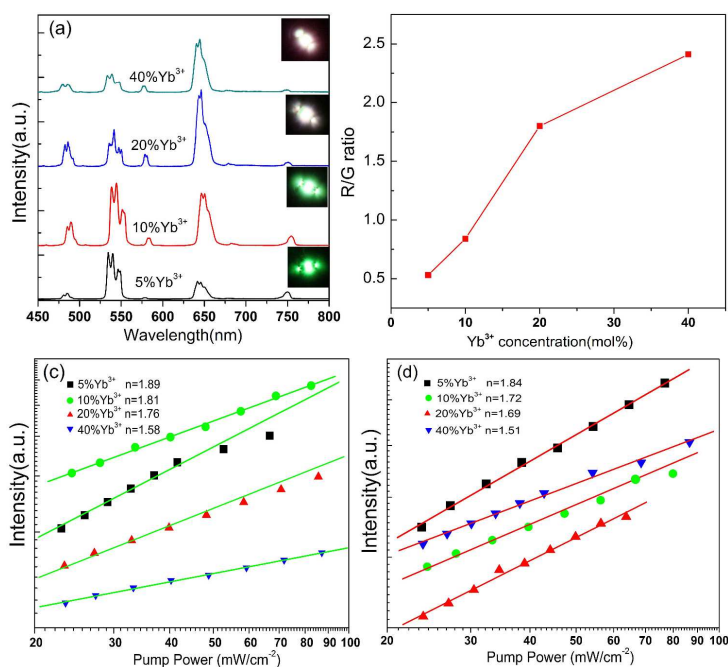Fig. 8 (a) UC emission spectra and (b) R/G ratio of single $NaYF_4$: $x\%Yb^{3+}/2\%Ho^{3+}$ microrods with different Yb^{3+} concentration (x=5, 10, 20, 40) under 980 nm excitation. The inset shows the corresponding luminescence photograph. Pump power dependence of the green (c) and red (d) UC emission of single $NaYF_4$: Yb^{3+}/Ho^{3+} microrods with different Yb^{3+} concentration.
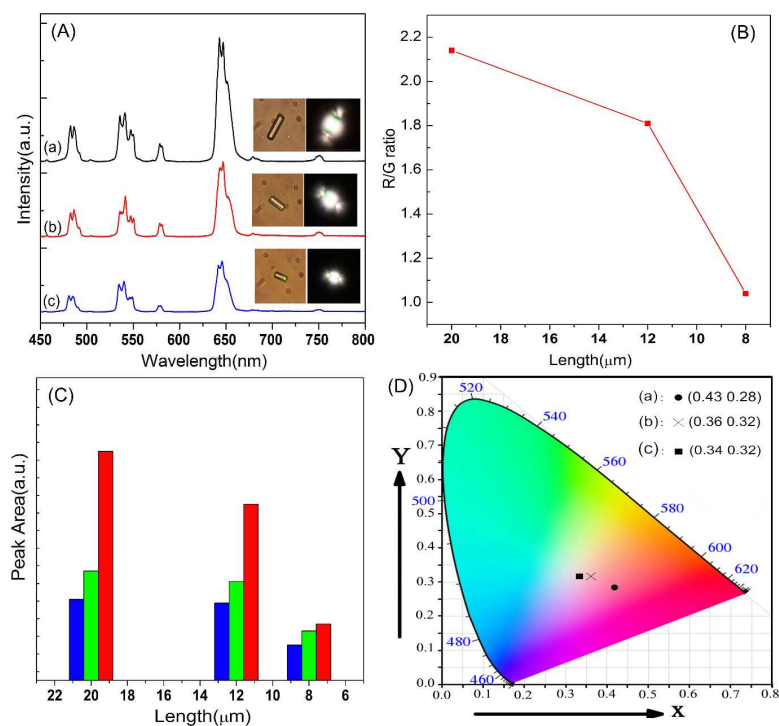
Fig. 9   UC emission spectra (A), R/G ratio (B), the peak area of the blue, green and red emission (C) and CIE chromaticity diagram (D) of a single NaYF$_4$: Yb^{3+}/Ho^{3+} microrod as a function of particle size (length) (a) 20 μm, (b) 12 μm, (c) 8 μm. The insets show the corresponding luminescence photographs
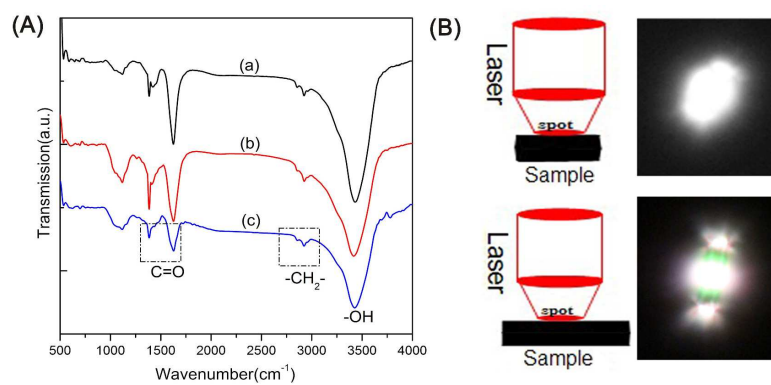

Fig. 10   (A) FTIR spectra of a single NaYF$_4$: Yb^{3+}/Ho^{3+} microrod as a function of particle size (length) (a) 20 μm, (b) 12 μm, (c) 8 μm. (B) Schematic diagram of the excitation of single microrod with different size.